



RESEARCH LETTER

10.1029/2023GL103203

Electron Acceleration by Interaction of Two Filamentary Currents Within a Magnetopause Magnetic Flux Rope

Shimou Wang^{1,2,3} , Rongsheng Wang^{1,2,3} , Quanming Lu^{1,2,3} , J. L. Burch⁴, Ian J. Cohen⁵ , A. N. Jaynes⁶ , and R. E. Ergun⁷

Key Points:

- Two types of filamentary currents (FCs) were observed near the center of a magnetic flux rope
- Stochastic electric fields were generated inside two FCs and accelerated electrons
- Electrons were accelerated up to 200 keV in the compressed region between two currents by the betatron mechanism

¹Deep Space Exploration Laboratory, School of Earth and Space Sciences, University of Science and Technology of China, Hefei, China, ²CAS Center for Excellence in Comparative Planetology, CAS Key Laboratory of Geospace Environment, Anhui Mengcheng National Geophysical Observatory, University of Science and Technology of China, Hefei, China, ³Collaborative Innovation Center of Astronautical Science and Technology, Harbin, China, ⁴Southwest Research Institute, San Antonio, TX, USA, ⁵The Johns Hopkins University Applied Physics Laboratory, Laurel, MD, USA, ⁶Department of Physics and Astronomy, University of Iowa, Iowa City, IA, USA, ⁷Laboratory of Atmospheric and Space Sciences, University of Colorado, Boulder, CO, USA

Correspondence to:

R. Wang and Q. Lu,
rswan@ustc.edu.cn;
qmlu@ustc.edu.cn

Citation:

Wang, S., Wang, R., Lu, Q., Burch, J. L., Cohen, I. J., Jaynes, A. N., & Ergun, R. E. (2023). Electron acceleration by interaction of two filamentary currents within a magnetopause magnetic flux rope. *Geophysical Research Letters*, 50, e2023GL103203. <https://doi.org/10.1029/2023GL103203>

Received 13 FEB 2023
Accepted 18 MAY 2023

Abstract Two types of filamentary currents (FCs) were observed inside a magnetic flux rope at the magnetopause by the Magnetospheric Multiscale mission. The first FC is identified as an electron vortex, while the other is a reconnecting current sheet. Stochastic electric fields were generated within the FCs, resulting in electron acceleration up to a few keV, similar to recent simulations of electron acceleration inside vortex, which is a second-order Fermi acceleration. Furthermore, two FCs propagated at different speeds, causing compression in the region between them. Energetic electrons up to 200 keV were detected in the compressed region and displayed a double power-law spectrum. Observations suggest that the electrons were mainly accelerated by betatron mechanism in the compressed region. The formation, evolution, and interaction of FCs provide a novel mechanism for electron acceleration. These results clearly show the significance of electron-scale dynamics within flux rope.

Plain Language Summary Magnetic reconnection is a fundamental plasma process by which magnetic energy is converted into the kinetic energy of charged particles. Understanding the acceleration mechanisms for the energetic electrons during magnetic reconnection is a long-standing question in the study of space and astrophysical plasmas. Using Magnetospheric Multiscale observations at Earth's magnetopause, we present in situ evidence of electron acceleration up to 200 keV between two consecutive filamentary currents (FCs) inside a magnetic flux rope. Two FCs propagate at different speeds, with the second moving faster, thus causing a compressed region between them. These results provide an important new way for electron acceleration in magnetic reconnection.

1. Introduction

Magnetic reconnection is a fundamental plasma process that explosively converts magnetic energy into plasma kinetic energy and produces energetic electrons in various plasma environments (Yamada et al., 2010). Observations in the solar atmosphere (Benz, 2017; Lin, 2011) and the Earth's magnetosphere (X. Li et al., 2022; Oieroset et al., 2002; Oka et al., 2016) indicate that these energetic electrons generally have a power-law distribution. Understanding the acceleration mechanisms for these electrons is a long-standing question in the study of reconnection. Previous studies have shown that flux ropes (FRs) or magnetic islands in two-dimensional cases likely play a critical role in accelerating electrons (Chen et al., 2008; Drake et al., 2006; Fu et al., 2006; Lu et al., 2020; Sironi & Spitkovsky, 2014; R Wang et al., 2010; Zank et al., 2014). It has been proposed that electrons can be trapped in a magnetic island bounded by two X-lines and gain energy through curvature and gradient drift acceleration during island contraction (Kliem, 1994). For a system of volume-filling islands, electrons undergo repetitive acceleration and scattering between randomly distributed islands, leading to a stochastic acceleration process (Drake et al., 2006). Electrons can also be accelerated by the electric field generated during the magnetic island merging (Oka et al., 2010; Zank et al., 2014). Recent simulations have used a guiding-center theory to assess the contributions of curvature drift, gradient drift, and parallel electric fields to electron acceleration during reconnection (Dahlin et al., 2014; Guo et al., 2015; X. Li et al., 2015). A similar approach has been used to study electron acceleration within FRs observed in the Earth's magnetosphere (S Wang et al., 2021; Zhong et al., 2020).

© 2023 The Authors.

This is an open access article under the terms of the [Creative Commons Attribution-NonCommercial License](https://creativecommons.org/licenses/by-nc/4.0/), which permits use, distribution and reproduction in any medium, provided the original work is properly cited and is not used for commercial purposes.

Nevertheless, there has recently been increasing interest in fine structures of FRs and associated electron acceleration owing to high-time resolution measurements from the Magnetospheric Multiscale (MMS) mission (Burch et al., 2016). MMS observations at the magnetopause found multiple filamentary currents (FCs) within the FRs (Eastwood et al., 2016; R Wang et al., 2017). The fragmented FCs can be produced by various instabilities (Che et al., 2011; Daughton et al., 2011; Huang et al., 2017; Price et al., 2016). Particle-in-cell simulations have shown that secondary reconnection in fragmented current sheets can accelerate electrons by parallel electric fields (Huang et al., 2017). In situ observations also demonstrate that FCs inside FRs are secondary reconnection sites and cause net magnetic energy dissipation (S Wang et al., 2020). In the magnetotail, some electron-scale structures like vortices (Stawarz et al., 2018) observed in FRs are thought to be novel acceleration regions. Recent simulations (Che & Zank, 2020; Che et al., 2021) proposed that electrons can be accelerated inside vortices during reconnection with a large guide field. The randomly distributed inductive electric field generated by the vortices expansion leads to the stochastic acceleration of electrons and produces a power-law distribution with an index of 3.5. This new acceleration mechanism by multi-vortices is thought to be efficient in explaining energetic electrons produced in solar flares (Che & Zank, 2020). While these studies imply that filamentary structures inside FRs may contribute to electron acceleration, direct evidence of them remains scarce.

In this letter, we report the first in situ observations of electron acceleration between two consecutive FCs within a FR. The electrons were accelerated up to 200 keV and displayed a double power-law spectrum. Data from several instruments of the MMS mission including the Fluxgate Magnetometer (Russell et al., 2016), the Electric Double Probes (Ergun et al., 2016; Lindqvist et al., 2016), the Fast Plasma Investigation (Pollock et al., 2016), and the Fly's Eye Energetic Particle Spectrometer (Blake et al., 2016) are used.

2. Event Overview

Figures 1a–1f show MMS1 observations during 00:24:40–00:26:30 UT on 20 February 2016 in Geocentric Solar Ecliptic coordinates. MMS1 was located at (4.5, -10.5 , -1.1) R_E and traversed the dawn flank magnetopause from 00:26:05 to 00:26:13 UT. The crossing is characterized by changes in the electron energy spectrum (Figure 1a), magnetic field B_z (Figure 1c), and plasma density (Figure 1d). Before \sim 00:25:45 UT, MMS1 was in the magnetosheath. Between two vertical black dashed lines, MMS1 observed a bipolar B_y variation and associated $|\mathbf{B}|$ enhancement, suggesting a FR crossing. The total pressure had a peak at the FR center (Figure 1f). This is another typical signature of FRs in which the pressure force is balanced by the magnetic tension force (Hasegawa et al., 2023; Hwang et al., 2016). A striking feature inside this FR is that energetic electron (47–214 keV) fluxes increased by an order of magnitude at \sim 00:25:03 UT abruptly (Figure 1b). The energetic electron flux enhancement in such a localized region near the FR center is a novel observation.

To analyze the properties of the FR, the data are transformed into a local FR coordinate system (abbreviated as ijk) determined by minimum variance analysis (Sonnerup & Scheible, 1998) of the MMS1 magnetic field data between 00:24:57 and 00:25:07 UT. Here, $\mathbf{i} = (-0.382, 0.834, 0.399)_{\text{GSE}}$, $\mathbf{j} = (-0.223, 0.335, -0.915)_{\text{GSE}}$, and $\mathbf{k} = (-0.897, -0.439, 0.058)_{\text{GSE}}$. Figures 1g–1k present an enlarged view of the FR. A correlated increase in $|\mathbf{B}|$ and $|B_j|$ peaked at the reversal point of bipolar B_i variation (Figure 1g). The ion flows were stable and mainly in $+k$ direction (Figure 1h), with an average value of \sim 203.3 km/s. Four-spacecraft timing analysis (Schwartz, 1998) based on B_i reveals that the FR moved along $(-0.310, 0.195, 0.931)_{ijk}$ direction with a speed of 154.7 km/s. The cross-section diameter of the FR is thus \sim 2011.1 km (\sim 33.6 d_i), where ion inertial length d_i is 59.9 km determined from the background density of 14.5 cm^{-3} . At the FR center, two conspicuous electron flows were present (Figure 1i) and largely distinguished from ambient stable flows. Two FCs, corresponding to current spikes, were mainly carried by the electrons, and the perpendicular component was comparable to the parallel current (Figure 1j). Simultaneously, two electric field spikes were found (Figure 1k). These local plasma and field variations suggest that some electron-scale processes were occurring therein.

3. Analysis of Two Filamentary Currents

Figures 2a–2l and 2m–2x show a zoom-in of two FCs (labeled as FC1 and FC2) respectively. The magnetic field, electric field, and particle moments data used in Figure 2 are averaged over four MMS satellites. As the FR coordinate system (ijk) is determined over a long interval (10 s), it may not be suitable for local and smaller-scale FCs. Therefore, a new coordinate system (LMN) for each of FCs is determined by a hybrid method as discussed

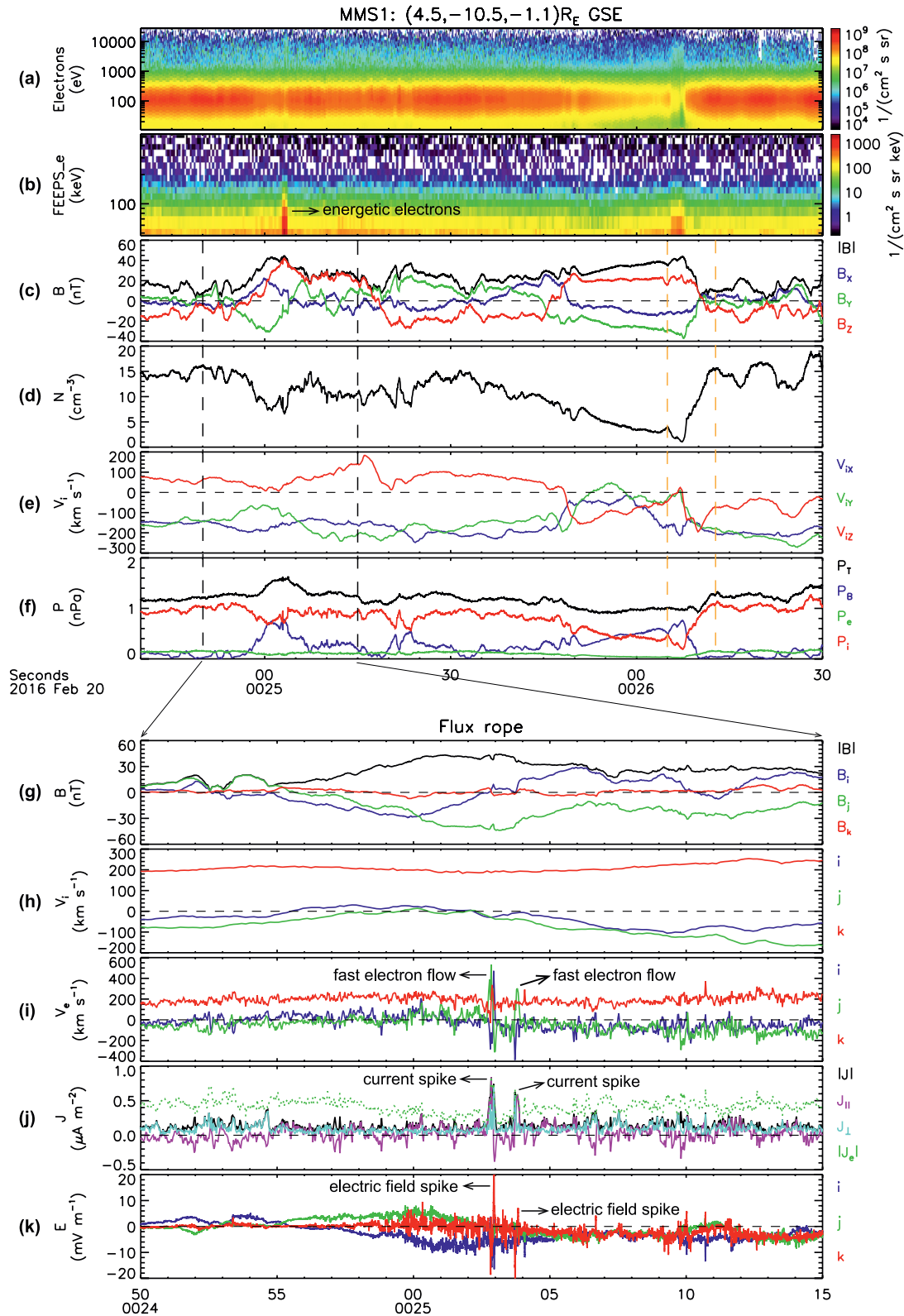


Figure 1. (a, b) Energy-time spectrograms of electrons measured by Fast Plasma Investigation and Fly's Eye Energetic Particle Spectrometer instruments. (c) Magnetic field. (d) Electron density. (e) Ion flows. (f) Total, magnetic, electron, and ion pressures. (g–k) Enlarged view of magnetic field, ion flow, electron flows, current density, and electric field inside the flux rope in ijk coordinates.

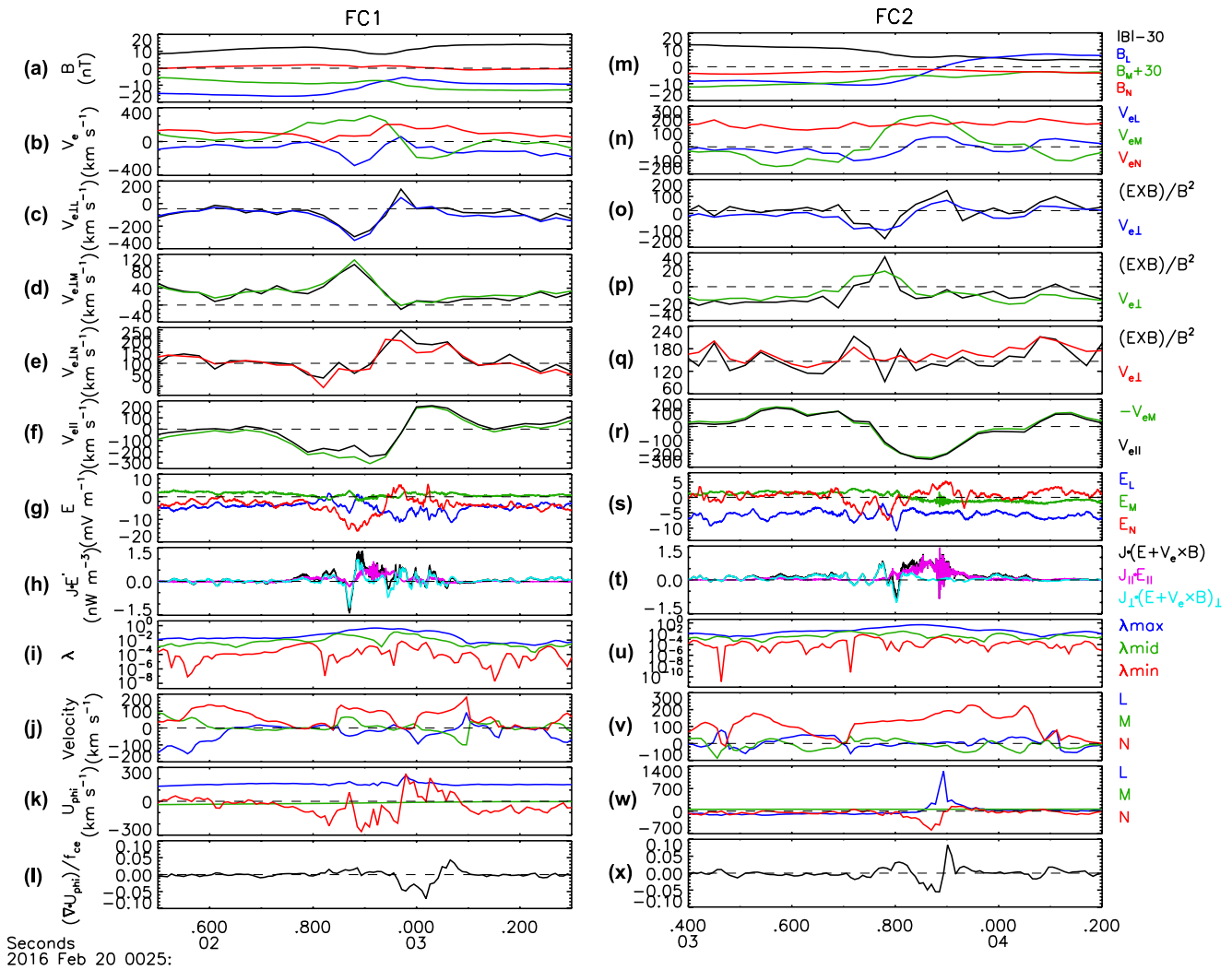


Figure 2. (a) Magnetic field. (b) Electron flows. (c–e) Three components of the perpendicular electron bulk velocity $\mathbf{V}_{e\perp}$ and $(\mathbf{E} \times \mathbf{B})/B^2$ drift velocity. (f) Parallel electron flows. (g) Electric field. (h) $\mathbf{J} \cdot (\mathbf{E} + \mathbf{V}_e \times \mathbf{B})$. (i) Eigenvalues from the minimum directional derivative method. (j) Structure velocity from the spatial-temporal difference method. (k) Magnetic flux transport velocity \mathbf{U}_{phi} . (l) $\nabla \cdot \mathbf{U}_{\text{phi}}$ normalized to the local electron cyclotron frequency. (m–x) are in the same format as (a–l).

by Denton et al. (2018). Note that the LMN coordinate system is different for two FCs. For FC1, $\mathbf{L} = (0.218, 0.975, -0.043)_{\text{GSE}}$, $\mathbf{M} = (-0.275, 0.020, -0.958)_{\text{GSE}}$, $\mathbf{N} = (-0.936, 0.222, 0.273)_{\text{GSE}}$; for FC2, $\mathbf{L} = (-0.707, 0.695, 0.130)_{\text{GSE}}$, $\mathbf{M} = (-0.019, 0.165, -0.986)_{\text{GSE}}$, $\mathbf{N} = (-0.707, -0.700, -0.104)_{\text{GSE}}$. The \mathbf{M} directions of two FCs almost coincide with \mathbf{j} direction (a rough estimate of the FR axis). The angle between the normal directions of two FCs is 61° .

3.1. Identification of Electron Vortex

Inside FC1, MMS observed a B_L rotation from ~ -16 nT to ~ -6 nT and a subsequent variation to ~ -9 nT between 00:25:02.8 and 00:25:03.1 UT (Figure 2a), corresponding to negative-to-positive J_M variation which is produced by the fast electron flow V_{eM} (Figure 2b). $|\mathbf{B}|$ is subtracted by 30 nT and shows a dip near FC1 center due to the decrease of $|B_M|$. The minimum directional derivative (MDD) method and spatial-temporal difference (STD) method (Shi et al., 2005, 2006) are used to estimate the dimensionality and propagation velocity of FC1. MDD method provides three directions of maximum, intermediate, and minimum variations of the magnetic field. Three eigenvalues are used as indicators of the structure dimensionality, as shown in Figure 2i. We can find $\lambda_{\text{max}} \gg \lambda_{\text{mid}}, \lambda_{\text{min}}$ or $\lambda_{\text{max}}, \lambda_{\text{mid}} \gg \lambda_{\text{min}}$ inside FC1, which shows a transition between 1-D (flattened) and 2-D (circular). STD method calculates the instantaneous velocity of a quasi-stationary structure and its result

is shown in Figure 2j. For FC1, the structure in the interval between 00:25:02.85 and 00:25:02.95 UT can be considered quasi-1D, with the leading part moving faster than the trailing part, implying an expanding nature (Yao et al., 2020). The thickness of this structure along N direction is calculated to be 10.6 km, ~ 5.9 local electron inertial lengths d_e . Outside of this interval, the structure transformed into the quasi-2D or quasi-3D, and the propagation velocity (Figure 2j) which assumes a 1D structure is not reliable.

The variation of electron flows inside FC1 seems weakened in Figure 2b as they are averaged over four satellites. If background velocity is subtracted (averaged between 00:25:02.6 and 00:25:02.7 UT), all three components of \mathbf{V}_e changed signs within FC1, indicating the possible existence of an electron vortex. The flow reversals are more clearly seen in Figures 2c–2f. Figures 2c–2e plot three components of perpendicular electron bulk velocity $\mathbf{V}_{e\perp}$ and $(\mathbf{E} \times \mathbf{B})/B^2$ drift velocity. The profiles of $\mathbf{V}_{e\perp}$ and $(\mathbf{E} \times \mathbf{B})/B^2$ match each other well except for some short intervals. In contrast to the perpendicular flow, the field-aligned flow $V_{e\parallel}$ was almost identical to $-V_{eM}$ and reversed from negative to positive at $\sim 00:25:02.98$ UT (Figure 2f).

The electron velocity variations are further analyzed by taking advantage of four-point MMS measurements (Figures 3d and 3e), and the velocity projection in the LN plane is displayed in Figure 3f. The black, red, green, and blue diamonds in Figure 3f represent the relative positions of four satellites in the LN plane. The arrows with different colors present velocity vectors at different times during the interval of flow reversal. $(\mathbf{E} \times \mathbf{B})/B^2$ velocity with higher resolution is used to assess the variations of V_{eL} and V_{eN} with background velocity removed. The gray dashed arrows represent the MMS path through FC1 based on the STD result. One can see a clear clockwise electron vortex in the LN plane, not a velocity shear layer. Then, an anticlockwise current loop, mainly carried by the electrons, could generate a positive B_M (Figure 3b). Note that MMS3 observed a weaker positive B_M inside FC1, consistent with the fact that MMS3 crossed the edge of the vortex. Although the flow shear along M direction was also large, a vortex could not be generated in this direction since the B_M component was large.

Figure 2h plots the energy conversion rate in the electron's rest frame $\mathbf{J} \cdot (\mathbf{E} + \mathbf{V}_e \times \mathbf{B})$ (Zenitani et al., 2011) and its contribution from parallel and perpendicular components. Some large positive and negative $\mathbf{J}_\perp \cdot (\mathbf{E} + \mathbf{V}_e \times \mathbf{B})_\perp$ are seen inside FC1, and the net effect is about zero. Moreover, a positive $\mathbf{J}_\parallel \cdot \mathbf{E}_\parallel$ existed through FC1, indicating that magnetic energy was being converted into electron energy by E_\parallel . Inside both FCs, \mathbf{J} was nearly equal to \mathbf{J}_e .

3.2. Identification of Reconnecting Current Sheet

Since FC2 was observed in proximity to FC1, a similar analysis is performed for FC2 in Figures 2m–2x and 3g–3l. Some differences are found. First, FC2 can be regarded as a quasi-1D current sheet with $\lambda_{\max} \gg \lambda_{\text{mid}}, \lambda_{\min}$ (Figure 2u) during the whole interval of B_L reversal from negative to positive (Figure 2m). The current sheet has a magnetic shear of 28° . The STD result suggests that its leading part was moving slower than trailing part. So the current sheet was being compressed. Its thickness is estimated to be 40.8 km, ~ 0.6 local ion inertial length. Electron vectors projected onto the LN plane show a disordered variation (Figure 3l). Fast electron flow V_{eM} produced the main current J_M and associated reversal of B_L . Inside the current sheet, MMS observed a positive electron jet in L direction at the B_L reversal point. However, it is difficult to identify whether this sub-ion-scale current sheet with enhanced jet was reconnecting, since the shear flow inside FC2 may distort the reconnection signatures. Therefore we use the magnetic flux transport (MFT) analysis here (T Li et al., 2021). This method can identify active reconnection site by clear inward and outward MFT around the X-point and a quadrupolar structure in the divergence of MFT. The signatures associated with the MFT velocity remain well even in strong background shear flows. Qi et al. (2022) examined the MFT in those reported reconnection events using MMS data and showed this method can successfully identify reconnection.

Figures 2w and 2x show the MFT velocity U_{phi} and its divergence. U_{phi} is defined as

$$\mathbf{U}_{\text{phi}} \equiv \mathbf{v}_{ep} - (\mathbf{v}_{ep} \cdot \mathbf{b}_p) \mathbf{b}_p + \frac{\mathbf{E}'_M}{B_p} (\mathbf{M} \times \mathbf{b}_p),$$

where $\mathbf{b}_p = \mathbf{B}_p/|\mathbf{B}_p|$ is the unit vector of the magnetic field component in the LN plane, \mathbf{v}_{ep} is the electron flow in the LN plane, \mathbf{M} is the out-of-plane direction, $\mathbf{E}' = \mathbf{E} + \mathbf{v}_e \times \mathbf{B}$. U_{phi} presents a bipolar variation in N direction and a unipolar peak in +L direction. The MFT outflow velocity is larger than 1,200 km/s, $\sim 0.5 V_{AeL}$. The bidirectional MFT inflows and unidirectional outflow are consistent with the MMS crossing of +L side of the X-line. A bipolar signature in $\nabla \cdot \mathbf{U}_{\text{phi}}$ is also consistent with converging MFT inflows and diverging outflows near the X-line.

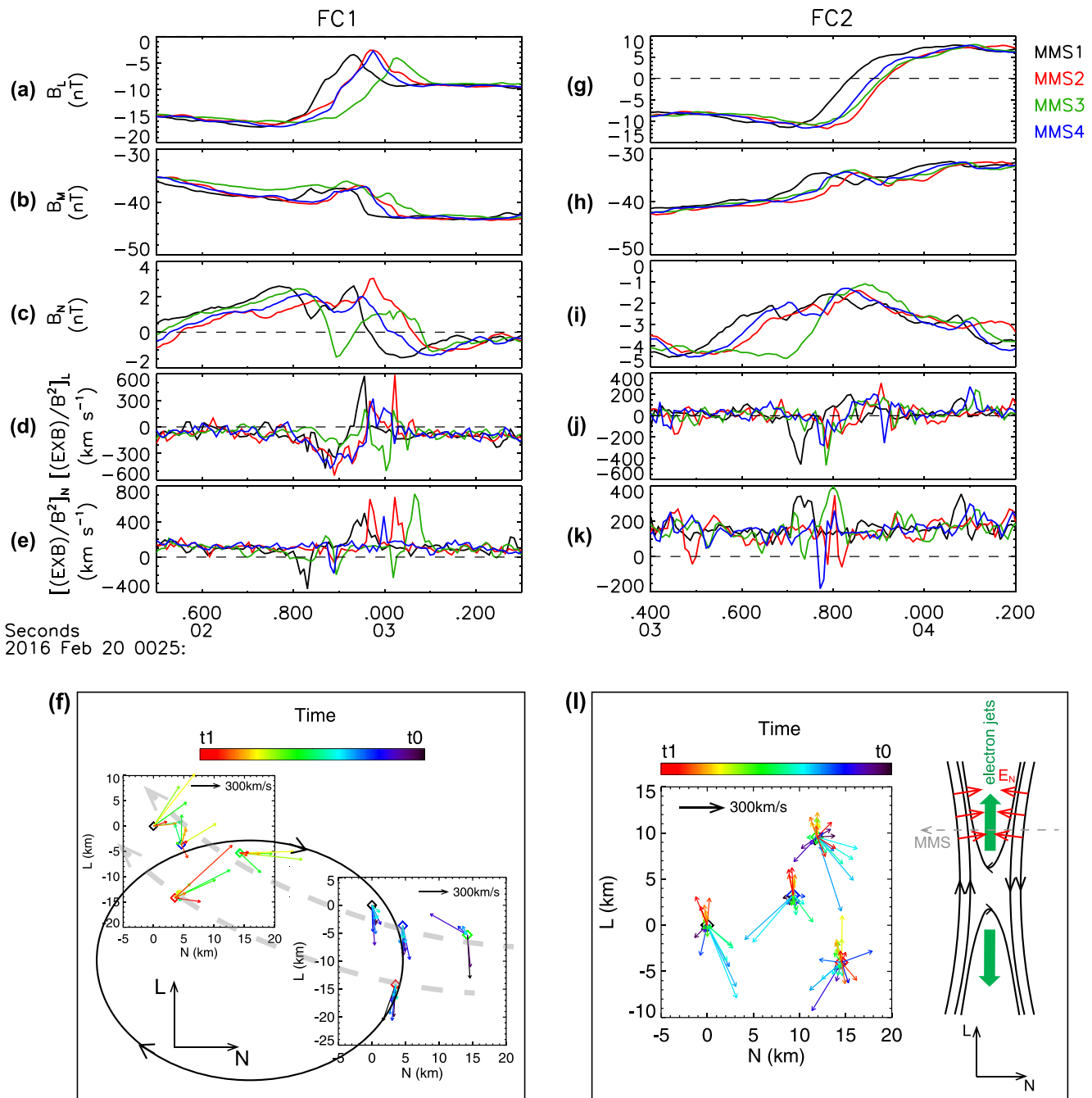


Figure 3. (a–c) Magnetic field observed by four satellites. (d, e) L and N components of the $(\mathbf{E} \times \mathbf{B})/B^2$ drift velocity observed by four satellites. (f) Projection of the velocity in the LN plane observed at four satellites at different times. (g–l) are in the same format as (a–f).

The MFT signatures suggest that MMS was crossing a reconnecting current sheet on the $+L$ side, as shown in a schematic of reconnection in a current sheet (Figure 3i). Magnetic field B_N was persistently negative throughout the FC2 encounter, consistent with the interpretation of crossing a reconnecting current sheet on the $+L$ side of the X-line. Electric field E_N shows a negative-to-positive variation (Figure 2s), pointing toward the current sheet center. Note that electric field E_M has a negative enhancement at the reconnecting site. This reconnection electric field is used to derive a normalized reconnection rate $R = E_M/(V_{Ae}B_L)$ which is estimated to be ~ 0.1 , similar to previous studies (Burch et al., 2020; Liu et al., 2017). Moreover, $\mathbf{J} \cdot (\mathbf{E} + \mathbf{V}_e \times \mathbf{B})$ is positive and dominated by $\mathbf{J}_{\parallel} \cdot \mathbf{E}_{\parallel}$ inside the current sheet, suggesting energy conversion from magnetic field to electrons. Based on these signatures and estimates, FC2 is identified as an active reconnecting current sheet. There was no ion outflow

or heating inside the current sheet, suggesting an electron-only reconnection, similar to that discovered in the magnetosheath (Phan et al., 2018).

For comparison, the MFT velocity and its divergence are also calculated in FC1 (Figures 2k and 2l). There is no MFT outflow inside FC1, and the divergence of the MFT has a bipolar variation but with a small value ($<0.05 f_{ce}$) on the positive side, suggesting that MMS did not cross a reconnection site.

Based on the analysis above, two FCs present different observational characteristics. FC1 is identified as an expanding electron vortex, while FC2 is a reconnecting current sheet. From the STD method, we note that FC1 propagated with an average speed of 108 km/s along $(-0.99, 0.00, 0.11)_{GSE}$, and FC2 propagated with 163 km/s along $(-0.71, -0.70, -0.07)_{GSE}$, tilted $\sim 46^\circ$ to x_{GSE} . Thus the STD results suggest that FC1 propagated slower than FC2.

4. Electron Acceleration Associated With Filamentary Currents

Figure 4 shows electron pitch angle distributions (ePADs) around two FCs. Next, we will discuss the electron acceleration within and between FCs. Inside two FCs, MMS observed enhanced fluxes at energies <2 keV (Figure 4b), mainly in the parallel or antiparallel direction (Figures 4f and 4g). The vertical striping in Figures 4f–4h is caused by some instrument artifact and does not affect our main conclusion. Further examination shows there is a good correspondence between polarities of E_{\parallel} (Figure 4d) and ePADs of these electrons. Therefore, these field-aligned electrons were directly accelerated by E_{\parallel} . Assuming that E_{\parallel} is distributed along the field line with an average amplitude of 2 mV/m, it would extend over 950 km to accelerate electrons from 100 eV to 2 keV. This distance also provides an estimate of the vortex extension along the axis.

The observed E_{\parallel} inside FC1 could be induced by vortex expansion as the simulations suggested (Che & Zank, 2020). As the vortex is in the LN plane perpendicular to the FR axis, the electric field induced by the vortex should be along the axis. The axial magnetic field is the dominant component inside the vortex, therefore the observed E_{\parallel} is nearly parallel to the axial magnetic field. Note that E_{\parallel} observed by four satellites had different variations (not shown), suggesting a complex distribution inside FC1. It is consistent with the simulations in which the turbulent magnetic fields inside the vortex induce randomly localized electric fields (Che & Zank, 2020). Inside FC2, MMS observed a positive E_{\parallel} which is identified as the reconnection electric field near the X-point. This unipolar E_{\parallel} was also accompanied by intense fluctuations indicating a turbulent state, similar to that inside FC1.

Between FC1 and FC2, energetic electrons (2–200 keV, about 3–300 times the thermal energy) fluxes increased by an order of magnitude between 00:25:03.0 and 00:25:03.7 UT than those outside this region. Figure 4j compares the electron energy spectra between two FCs (magenta line), within FC2 (cyan line), outside the FCs (black line), in the magnetosheath (green line), and in the magnetosphere (blue line). The black line is a combination of the green and blue lines, suggesting that the electron population inside the FR is a mixture of magnetosheath and magnetospheric electrons. The comparison shows that at energies above 2 keV the phase space density (PSD) of electrons between two FCs is higher than that outside FCs. These accelerated electrons display a double power-law distribution with an index of 3.70 in the energy range of 8–85 keV and 8.07 in 103–248 keV. The index of 3.70 is similar to that (3.50) observed in the entire simulation domain with multiple vortices (Che & Zank, 2020). The energy of electrons with a power-law distribution in the simulations increases to 10–100 times the thermal energy, corresponding to about 7–70 keV in our event, which agrees well with the observations. Therefore, the electrons in 8–85 keV could be accelerated by the stochastic electric fields within FCs and then drift into the region between FCs. The spectrum in 103–248 keV has an index of 8.07, different from that for the lower-energy electrons. This suggests that energetic electrons in 103–248 keV can be accelerated by other mechanisms. The electron spectrum within FC2 (cyan line) is also plotted in Figure 4j. The PSD of electrons in 0.1–10 keV is larger than that outside the FCs, with a similar spectrum to that between two FCs. Note that the spectrum within FC2 does not show a power-law distribution in 8–85 keV and decreases significantly above ~ 10 keV. It is probably due to the small size of the FC2 (40.8 km) which is comparable to the gyroradius of 10 keV electrons (9.1 km), and thus electrons cannot be fully accelerated to a power-law distribution. The electron spectrum within FC1 is nearly identical to that within FC2 in 0.1–1 keV and then decreases significantly, corresponding to a smaller scale of FC1 (10.6 km).

Another important question is how the electrons in 103–248 keV were accelerated between two FCs. These observed energetic electrons could be accelerated from the preaccelerated electrons within FCs. Another

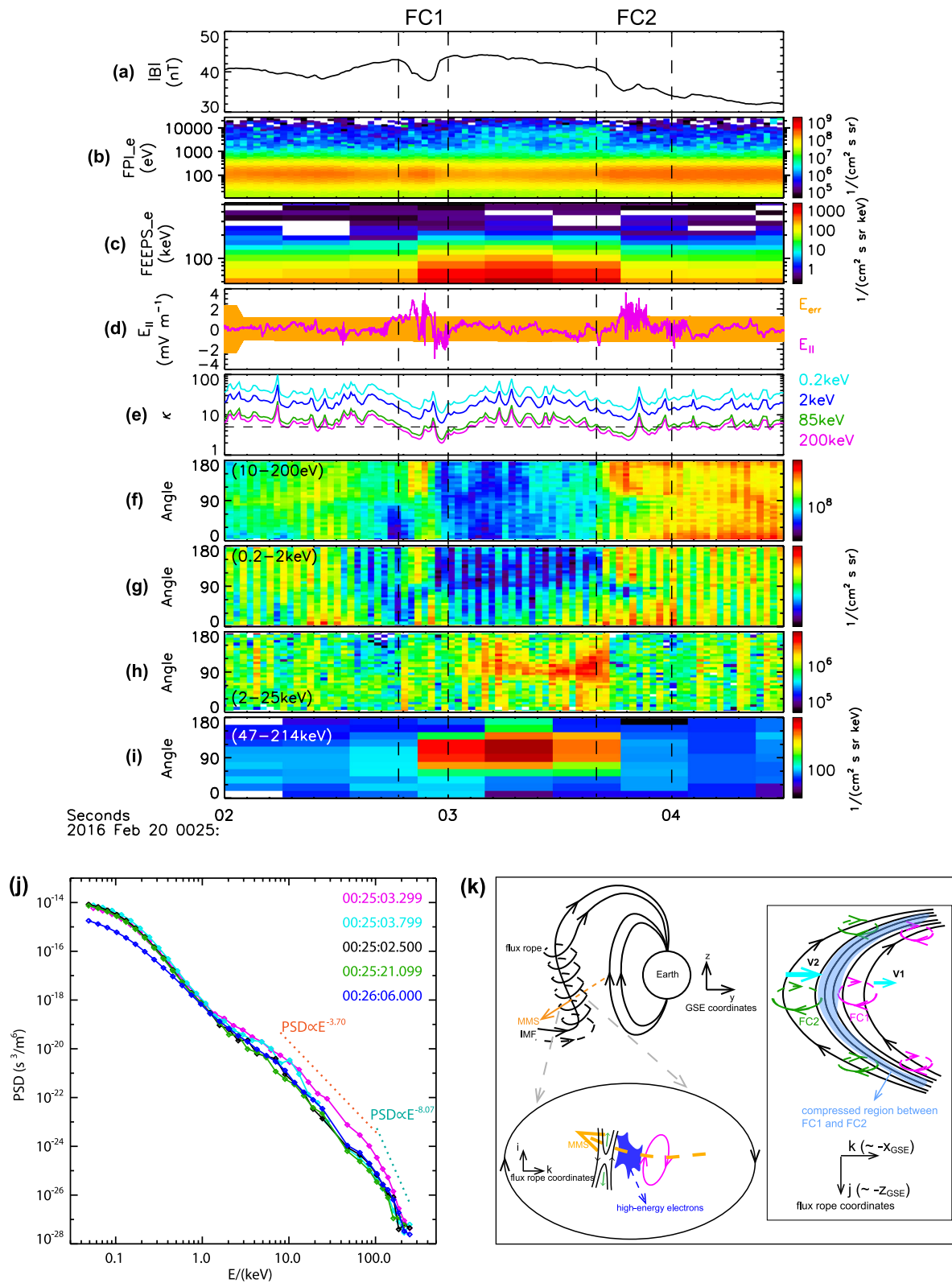


Figure 4. (a) Magnetic field. (b, c) Energy-time spectrograms of electrons. (d) Parallel electric field. (e) Adiabatic parameter κ . (f–i) Electron pitch angle distributions. (j) Electron energy spectra in the compressed region (magenta line), within FC2 (cyan line), within the flux rope but outside the compressed region (black line), in the magnetosheath (green line), and in the magnetosphere (blue line). (k) A sketch summarizing the main structures and processes.

possibility is that they were accelerated electrons of magnetospheric origin since they were observed in the region of large and positive B_z and low density. Figure 4e shows the adiabatic parameter κ at four different energies, where κ is the square root of the ratio between the magnetic field curvature radius and the Larmor radius (Büchner & Zelenyi, 1989). Electrons were adiabatic between two FCs because their κ were above 5. As shown in Section 3, FC1 propagated slower than FC2, thus FC1 may seem an obstacle for FC2. A possible scenario (right of Figure 4k) is that the interaction of FC1 and FC2 forms a compressed region (blue-shaded region) between them. This scenario has some similarities to the interaction of two jet fronts in the magnetotail (Catapano et al., 2021). As a result of motion of FCs, the length of the curved magnetic field decreases, leading to an increase in the energy of the trapped electrons via Fermi process due to the conservation of the longitudinal invariant. Betatron acceleration also plays a role in the compressed region, as there is an increase of $|\mathbf{B}|$. Both Fermi and betatron accelerations can affect the change in electron pitch angles. Therefore, when two mechanisms are at work simultaneously, the pitch angles of accelerated electrons are determined according to their relative importance. From Figures 4h and 4i, betatron acceleration should be the dominant mechanism through the compressed region. Fermi acceleration was weaker overall, probably because of small magnetic curvature. A more detailed analysis of Figure 4h reveals that electron flux in the 90° direction was the highest in the leading edge of the FC2, concurrent with nonadiabatic electron motion. Considering the strongly enhanced polarization electric fields E_N in the FC2 (Figure 2s), surfing acceleration in the reconnecting current sheet, as discussed by Hoshino (2005), may work to perpendicularly accelerate electrons therein.

5. Discussion and Conclusions

In this letter, we present the first in situ observations of electron acceleration associated with two FCs within a FR. Figure 4k provides a sketch summarizing the main structures and processes. FC1 is identified as an expanding electron vortex, almost frozen-in with $\mathbf{E} \times \mathbf{B}$ drifting electrons. MMS observed a complex E_{\parallel} distribution inside FC1, which exhibited an overall bipolar variation but was accompanied by intense fluctuations, suggesting that the induced E_{\parallel} is turbulent. Che and Zank (2020) proposed that the expansion of turbulent vortices can induce stochastic electric fields that are important for producing a power-law spectrum. The acceleration process inside FC1 is similar to the simulation results, although electrons cannot be accelerated to high energy inside it. This is probably due to the small scale of the vortex and that magnetic energy has not yet been dissipated in large quantities. In contrast, FC2 is identified as a reconnecting current sheet with a large guide field. The reconnection electric field in it was also accompanied by strong fluctuations. It appears that the turbulent inductive electric field is a common feature of FCs, but further study is needed to demonstrate this.

Another important result is that energetic electrons up to 200 keV were observed between two FCs and displayed a double power-law distribution, in which the lower-energy (8–85 keV) band has an index of 3.70 and the higher-energy (103–248 keV) band with 8.07. Since two FCs propagated at different velocities, with the second moving faster, the region between them was compressed. The electrons in 8–85 keV are found to be accelerated by stochastic electric fields inside FCs and then drift into the compressed region between FCs. For higher-energy electrons, they were accelerated in the compressed region by the betatron mechanism. This scenario is similar to the formation of a magnetic bottle between two jet fronts in the magnetotail (Birn et al., 2011; Catapano et al., 2021). However, in our event, the region between two FCs had enhanced magnetic fields and smaller spatial scale. Betatron acceleration is the dominant mechanism in this compressed region, as the accelerated electrons were mainly in the 90° direction.

In conclusion, we present MMS observations of two types of FCs and associated electron acceleration within and between them. These results suggest that electron acceleration in our event is not consistent with the acceleration at two ends of a contracting FR (Drake et al., 2006), but is closely related to FCs near the FR center. Recent observations in the heliospheric current sheet (Desai et al., 2022) present challenges for some reconnection-driven acceleration models like direct parallel electric fields and multi-islands acceleration. Our findings provide a new acceleration scenario that electrons can be accelerated by the stochastic electric fields within FCs and then drift into the compressed region between FCs in which they can be further accelerated to extremely high energy by the betatron mechanism. This study may help explain the particle acceleration associated with FRs with large scale and strong collisions in solar flares (Takasao et al., 2016).

Data Availability Statement

All the MMS data used in this work are available at the MMS data center (<https://lasp.colorado.edu/mms/sdc/public/about/browse-wrapper/>).

Acknowledgments

We thank the entire MMS team for providing such excellent and well calibrated data that permits this study. This work is supported by the B-type Strategic Priority Program of the Chinese Academy of Sciences (XDB41000000), the National Science Foundation of China (NSFC) Grants (41674143, 41922030, and 42174187), and the Fundamental Research Funds for the Central Universities.

References

- Benz, A. O. (2017). Flare observations. *Living Reviews in Solar Physics*, *14*, 1–59. <https://doi.org/10.1007/s41116-016-0004-3>
- Birn, J., Nakamura, R., Panov, E., & Hesse, M. (2011). Bursty bulk flows and dipolarization in MHD simulations of magnetotail reconnection. *Journal of Geophysical Research*, *116*(A1), A01210. <https://doi.org/10.1029/2010ja016083>
- Blake, J. B., Mauk, B. H., Baker, D. N., Carranza, P., Clemmons, J. H., Craft, J., et al. (2016). The Fly's Eye energetic particle spectrometer (FEEPS) sensors for the magnetospheric multiscale (MMS) mission. *Space Science Reviews*, *199*(1–4), 309–329. <https://doi.org/10.1007/s11214-015-0163-x>
- Büchner, J., & Zelenyi, L. M. (1989). Regular and chaotic charged particle motion in magnetotail-like field reversals: 1. Basic theory of trapped motion. *Journal of Geophysical Research*, *94*(A9), 11821–11842. <https://doi.org/10.1029/ja094ia09p11821>
- Burch, J. L., Moore, T. E., Torbert, R. B., & Giles, B. L. (2016). Magnetospheric multiscale overview and science objectives. *Space Science Reviews*, *199*(1–4), 5–21. <https://doi.org/10.1007/s11214-015-0164-9>
- Burch, J. L., Webster, J. M., Hesse, M., Genestreti, K. J., Denton, R. E., Phan, T. D., et al. (2020). Electron inflow velocities and reconnection rates at Earth's magnetopause and magnetosheath. *Geophysical Research Letters*, *47*(17), e2020GL089082. <https://doi.org/10.1029/2020gl089082>
- Catapano, F., Retino, A., Zimbardo, G., Alexandrova, A., Cohen, I. J., Turner, D. L., et al. (2021). In situ evidence of ion acceleration between consecutive reconnection jet fronts. *The Astrophysical Journal*, *908*(1), 73. <https://doi.org/10.3847/1538-4357/abce5a>
- Che, H., Drake, J. F., & Swisdak, M. (2011). A current filamentation mechanism for breaking magnetic field lines during reconnection. *Nature*, *474*(7350), 184–187. <https://doi.org/10.1038/nature10091>
- Che, H., & Zank, G. P. (2020). Electron acceleration from expanding magnetic vortices during reconnection with a guide field. *The Astrophysical Journal*, *889*(1), 11. <https://doi.org/10.3847/1538-4357/ab5d3b>
- Che, H., Zank, G. P., Benz, A. O., Tang, B., & Crawford, C. (2021). The formation of electron outflow jets with power-law energy distribution in guide-field magnetic reconnection. *The Astrophysical Journal*, *908*(1), 72. <https://doi.org/10.3847/1538-4357/abcf29>
- Chen, L. J., Bhattacharjee, A., Puhl-Quinn, P. A., Yang, H., Bessho, N., Imada, S., et al. (2008). Observation of energetic electrons within magnetic islands. *Nature Physics*, *4*(1), 19–23. <https://doi.org/10.1038/nphys777>
- Dahlin, J. T., Drake, J. F., & Swisdak, M. (2014). The mechanisms of electron heating and acceleration during magnetic reconnection. *Physics of Plasmas*, *21*(9), 092304. <https://doi.org/10.1063/1.4894484>
- Daughton, W., Roytershteyn, V., Karimabadi, H., Yin, L., Albright, B. J., Bergen, B., & Bowers, K. J. (2011). Role of electron physics in the development of turbulent magnetic reconnection in collisionless plasmas. *Nature Physics*, *7*(7), 539–542. <https://doi.org/10.1038/nphys1965>
- Denton, R., Sonnerup, B. Ö., Russell, C., Hasegawa, H., Phan, T. D., Strangeway, R., et al. (2018). Determining L-M-N current sheet coordinates at the magnetopause from Magnetospheric Multiscale data. *Journal of Geophysical Research: Space Physics*, *123*(3), 2274–2295. <https://doi.org/10.1002/2017ja024619>
- Desai, M., Mitchell, D., McComas, D., Drake, J., Phan, T., Szalay, J., et al. (2022). Suprathermal ion energy spectra and anisotropies near the heliospheric current sheet crossing observed by the Parker Solar Probe during encounter 7. *The Astrophysical Journal*, *927*(1), 62. <https://doi.org/10.3847/1538-4357/ac4961>
- Drake, J. F., Swisdak, M., Che, H., & Shay, M. A. (2006). Electron acceleration from contracting magnetic islands during reconnection. *Nature*, *443*(7111), 553–556. <https://doi.org/10.1038/nature05116>
- Eastwood, J. P., Phan, T. D., Cassak, P. A., Gershman, D. J., Haggerty, C., Malakit, K., et al. (2016). Ion-scale secondary flux ropes generated by magnetopause reconnection as resolved by MMS. *Geophysical Research Letters*, *43*(10), 4716–4724. <https://doi.org/10.1002/2016gl068747>
- Ergun, R. E., Tucker, S., Westfall, J., Goodrich, K. A., Malaspina, D. M., Summers, D., et al. (2016). The axial double probe and fields signal processing for the MMS mission. *Space Science Reviews*, *199*(1–4), 167–188. <https://doi.org/10.1007/s11214-014-0115-x>
- Fu, X. R., Lu, Q. M., & Wang, S. (2006). The process of electron acceleration during collisionless magnetic reconnection. *Physics of Plasmas*, *13*(1), 012309. <https://doi.org/10.1063/1.2164808>
- Guo, F., Liu, Y.-H., Daughton, W., & Li, H. (2015). Particle acceleration and plasma dynamics during magnetic reconnection in the magnetically dominated regime. *The Astrophysical Journal*, *806*(2), 167. <https://doi.org/10.1088/0004-637x/806/2/167>
- Hasegawa, H., Denton, R., Dokgo, K., Hwang, K. J., Nakamura, T., & Burch, J. (2023). Ion-scale magnetic flux rope generated from electron-scale magnetopause current sheet: Magnetospheric multiscale observations. *Journal of Geophysical Research: Space Physics*, *128*(3), e2022JA031092. <https://doi.org/10.1029/2022ja031092>
- Hoshino, M. (2005). Electron surfing acceleration in magnetic reconnection. *Journal of Geophysical Research*, *110*(A10), A10215. <https://doi.org/10.1029/2005ja011229>
- Huang, C., Lu, Q. M., Wang, R. S., Guo, F., Wu, M. Y., Lu, S., & Wang, S. (2017). Development of turbulent magnetic reconnection in a Magnetic Island. *The Astrophysical Journal*, *835*(2), 245. <https://doi.org/10.3847/1538-4357/835/2/245>
- Hwang, K. J., Sibeck, D. G., Giles, B. L., Pollock, C. J., Gershman, D., Avakov, L., et al. (2016). The substructure of a flux transfer event observed by the MMS spacecraft. *Geophysical Research Letters*, *43*(18), 9434–9443. <https://doi.org/10.1002/2016gl070934>
- Kliem, B. (1994). Particle orbits, trapping, and acceleration in a filamentary current sheet model. In *Paper presented at international astronomical union colloquium*. Cambridge University Press.
- Li, T. C., Liu, Y.-H., & Qi, Y. (2021). Identification of active magnetic reconnection using magnetic flux transport in plasma turbulence. *The Astrophysical Journal Letters*, *909*(2), L28. <https://doi.org/10.3847/2041-8213/abea0b>
- Li, X., Guo, F., Li, H., & Li, G. (2015). Nonthermally dominated electron acceleration during magnetic reconnection in a low- β plasma. *The Astrophysical Journal Letters*, *811*(2), L24. <https://doi.org/10.1088/2041-8205/811/2/L24>
- Li, X., Wang, R., Lu, Q., Russell, C. T., Lu, S., Cohen, I. J., et al. (2022). Three-dimensional network of filamentary currents and super-thermal electrons during magnetotail magnetic reconnection. *Nature Communications*, *13*(1), 3241. <https://doi.org/10.1038/s41467-022-31025-9>
- Lin, R. (2011). Energy release and particle acceleration in flares: Summary and future prospects. *Space Science Reviews*, *159*(1–4), 421–445. <https://doi.org/10.1007/s11214-011-9801-0>
- Lindqvist, P. A., Olsson, G., Torbert, R. B., King, B., Granoff, M., Rau, D., et al. (2016). The spin-plane double probe electric field instrument for MMS. *Space Science Reviews*, *199*(1–4), 137–165. <https://doi.org/10.1007/s11214-014-0116-9>
- Liu, Y.-H., Hesse, M., Guo, F., Daughton, W., Li, H., Cassak, P., & Shay, M. (2017). Why does steady-state magnetic reconnection have a maximum local rate of order 0.1? *Physical Review Letters*, *118*(8), 085101. <https://doi.org/10.1103/physrevlett.118.085101>
- Lu, S., Artemyev, A. V., Angelopoulos, V., & Pritchett, P. L. (2020). Energetic electron acceleration by ion-scale magnetic islands in turbulent magnetic reconnection: Particle-in-cell simulations and ARTEMIS observations. *The Astrophysical Journal*, *896*(2), 105. <https://doi.org/10.3847/1538-4357/ab908e>
- Oieroset, M., Lin, R. P., Phan, T. D., Larson, D. E., & Bale, S. D. (2002). Evidence for electron acceleration up to ~300 keV in the magnetic reconnection diffusion region of Earth's magnetotail. *Physical Review Letters*, *89*(19), 195001. <https://doi.org/10.1103/physrevlett.89.195001>

- Oka, M., Phan, T. D., Krucker, S., Fujimoto, M., & Shinohara, I. (2010). Electron acceleration by multi-island coalescence. *The Astrophysical Journal*, 714(1), 915–926. <https://doi.org/10.1088/0004-637x/714/1/915>
- Oka, M., Phan, T. D., Øieroset, M., & Angelopoulos, V. (2016). In situ evidence of electron energization in the electron diffusion region of magnetotail reconnection. *Journal of Geophysical Research: Space Physics*, 121(3), 1955–1968. <https://doi.org/10.1002/2015ja022040>
- Phan, T. D., Eastwood, J. P., Shay, M. A., Drake, J. F., Sonnerup, B. U. Ö., Fujimoto, M., et al. (2018). Electron magnetic reconnection without ion coupling in Earth's turbulent magnetosheath. *Nature*, 557(7704), 202. <https://doi.org/10.1038/s41586-018-0091-5>
- Pollock, C., Moore, T., Jacques, A., Burch, J., Gliese, U., Saito, Y., et al. (2016). Fast plasma investigation for magnetospheric multiscale. *Space Science Reviews*, 199(1–4), 331–406. <https://doi.org/10.1007/s11214-016-0245-4>
- Price, L., Swisdak, M., Drake, J. F., Cassak, P. A., Dahlin, J. T., & Ergun, R. E. (2016). The effects of turbulence on three-dimensional magnetic reconnection at the magnetopause. *Geophysical Research Letters*, 43(12), 6020–6027. <https://doi.org/10.1002/2016gl069578>
- Qi, Y., Li, T. C., Russell, C. T., Ergun, R. E., Jia, Y.-D., & Hubbert, M. (2022). Magnetic flux transport identification of active reconnection: Mms observations in Earth's magnetosphere. *The Astrophysical Journal Letters*, 926(2), L34. <https://doi.org/10.3847/2041-8213/ac5181>
- Russell, C. T., Anderson, B. J., Baumjohann, W., Bromund, K. R., Dearborn, D., Fischer, D., et al. (2016). The magnetospheric multiscale magnetometers. *Space Science Reviews*, 199(1–4), 189–256. <https://doi.org/10.1007/s11214-014-0057-3>
- Schwartz, S. J. (1998). Shock and discontinuity normals, mach numbers and related parameters. In G. Paschmann & P. W. Daly (Eds.), *Analysis methods for multi-spacecraft data* (pp. 249–270). International Space Science Institute.
- Shi, Q. Q., Shen, C., Dunlop, M. W., Pu, Z. Y., Zong, Q. G., Liu, Z. X., et al. (2006). Motion of observed structures calculated from multi-point magnetic field measurements: Application to Cluster. *Geophysical Research Letters*, 33(8), L08109. <https://doi.org/10.1029/2005gl025073>
- Shi, Q. Q., Shen, C., Pu, Z. Y., Dunlop, M. W., Zong, Q. G., Zhang, H., et al. (2005). Dimensional analysis of observed structures using multipoint magnetic field measurements: Application to Cluster. *Geophysical Research Letters*, 32(12), L12105. <https://doi.org/10.1029/2005gl022454>
- Sironi, L., & Spitkovsky, A. (2014). Relativistic reconnection: An efficient source of non-thermal particles. *The Astrophysical Journal Letters*, 783(1), L21. <https://doi.org/10.1088/2041-8205/783/1/L21>
- Sonnerup, B., & Scheible, M. (1998). *Analysis methods for multi-spacecraft data*. ISSI Scientific Report.
- Stawarz, J. E., Eastwood, J. P., Genestreti, K. J., Nakamura, R., Ergun, R. E., Burgess, D., et al. (2018). Intense electric fields and electron-scale substructure within magnetotail flux ropes as revealed by the magnetospheric multiscale mission. *Geophysical Research Letters*, 45(17), 8783–8792. <https://doi.org/10.1029/2018gl079095>
- Takasao, S., Asai, A., Isobe, H., & Shibata, K. (2016). Observational evidence of particle acceleration associated with plasmoid motions. *The Astrophysical Journal*, 828(2), 103. <https://doi.org/10.3847/0004-637x/828/2/103>
- Wang, R. S., Lu, Q., Nakamura, R., Baumjohann, W., Russell, C. T., Burch, J. L., et al. (2017). Interaction of magnetic flux ropes via magnetic reconnection observed at the magnetopause. *Journal of Geophysical Research: Space Physics*, 122(10), 10436–10447. <https://doi.org/10.1002/2017ja024482>
- Wang, R. S., Lu, Q. M., Du, A. M., & Wang, S. (2010). In situ observations of a secondary magnetic island in an ion diffusion region and associated energetic electrons. *Physical Review Letters*, 104(17), 175003. <https://doi.org/10.1103/physrevlett.104.175003>
- Wang, S. M., Wang, R. S., Lu, Q. M., Burch, J. L., & Wang, S. (2021). Energy dissipation via magnetic reconnection within the coherent structures of the magnetosheath turbulence. *Journal of Geophysical Research: Space Physics*, 126(4), e2020JA028860. <https://doi.org/10.1029/2020ja028860>
- Wang, S. M., Wang, R. S., Lu, Q. M., Fu, H. S., & Wang, S. (2020). Direct evidence of secondary reconnection inside filamentary currents of magnetic flux ropes during magnetic reconnection. *Nature Communications*, 11(1), 3964. <https://doi.org/10.1038/s41467-020-17803-3>
- Yamada, M., Kulsrud, R., & Ji, H. T. (2010). Magnetic reconnection. *Reviews of Modern Physics*, 82(1), 603–664. <https://doi.org/10.1103/revmodphys.82.603>
- Yao, S., Hamrin, M., Shi, Q., Yao, Z., Degeling, A., Zong, Q. G., et al. (2020). Propagating and dynamic properties of magnetic dips in the dayside magnetosheath: MMS observations. *Journal of Geophysical Research: Space Physics*, 125(6), e2019JA026736. <https://doi.org/10.1029/2019ja026736>
- Zank, G. P., le Roux, J. A., Webb, G. M., Dosch, A., & Khabarova, O. (2014). Particle acceleration via reconnection processes in the supersonic solar wind. *The Astrophysical Journal*, 797(1), 28. <https://doi.org/10.1088/0004-637x/797/1/28>
- Zenitani, S., Hesse, M., Klimas, A., & Kuznetsova, M. (2011). New measure of the dissipation region in collisionless magnetic reconnection. *Physical Review Letters*, 106(19), 195003. <https://doi.org/10.1103/physrevlett.106.195003>
- Zhong, Z. H., Zhou, M., Tang, R., Deng, X., Turner, D., Cohen, I., et al. (2020). Direct evidence for electron acceleration within ion-scale flux rope. *Geophysical Research Letters*, 47(1), e2019GL085141. <https://doi.org/10.1029/2019gl085141>